

## Article

# Thickness and Strength Analysis of Prestressed Anchor (Cable) Compression Arch Based on Safe Co-Mining of Deep Coal and Gas

Deyi Wu \*, Nanyu Li and Shuang Zhou

National-Local Joint Engineering Laboratory of Building Health Monitoring and Disaster Prevention Technology, College of Civil Engineering, Anhui Jianzhu University, Hefei 230601, China; linanyuyu@163.com (N.L.); 17718151061@163.com (S.Z.)

\* Correspondence: wudeyi136@163.com; Tel.: +86-151-5601-0510

**Abstract:** The stability of the gas extraction roadway is very important for the safe mining of coal and gas. The compression arch formed by the combined action of the prestressed bolt (cable) support and surrounding rock has been widely used in the engineering practice of the gas extraction roadway. It is of great engineering application value to analyze the influence of prestressed bolt (cable) parameters on the compression arch. In this paper, combined with the engineering practice of the deep roadway in Huainan and Huaibei mining area of Anhui Province, the mechanical parameters of surrounding rock are measured via field coring and the laboratory. The numerical simulation software FLAC<sup>3D</sup> is used to analyze the typical position of fractured mudstone, mudstone, sandy mudstone and muddy sandstone under the bolt pre-tightening force of  $F = 50$  kN, 70 kN and 100 kN; the bolt spacing of  $a \times b = 400$  mm  $\times$  400 mm, 500 mm  $\times$  500 mm and 600 mm  $\times$  600 mm; the bolt length of  $L = 1500$  mm, 2000 mm, 2600 mm and 3000 mm; and the distribution characteristics of additional compressive stress on the surface of the side. The influence of the different lithology and bolt parameters on the thickness and strength of the compression arch was analyzed, and on this basis, prestressed anchor cables with a pre-tightening force of  $F = 80$  kN, 100 kN and 120 kN and length of  $L = 3000$  mm, 4000 mm and 6000 mm were applied, and their influence on the thickness and strength of the compression arch was analyzed. The results show that the bolt pre-tightening force ( $F$ ) and the bolt length ( $L$ ) have a significant effect on the thickness of the compression arch, while the surrounding rock lithology, the bolt spacing ( $a \times b$ ), the anchor cable pre-tightening force ( $F$ ) and the anchor cable length ( $L$ ) have no obvious effect on the thickness of the compression arch. The surrounding rock lithology, the bolt pre-tightening force ( $F$ ), the bolt length ( $L$ ), the bolt spacing ( $a \times b$ ), the anchor cable pre-tightening force ( $F$ ) and the anchor cable length ( $L$ ) have a significant effect on the strength of the compression arch.



**Citation:** Wu, D.; Li, N.; Zhou, S. Thickness and Strength Analysis of Prestressed Anchor (Cable) Compression Arch Based on Safe Co-Mining of Deep Coal and Gas. *Sustainability* **2023**, *15*, 10716. <https://doi.org/10.3390/su151310716>

Academic Editors: Adam Smoliński and Dino Musmarra

Received: 24 April 2023

Revised: 25 June 2023

Accepted: 4 July 2023

Published: 7 July 2023

**Keywords:** gas safe mining; gas extraction roadway; prestressed bolt (cable); thickness of the compression arch; strength of the compression arch



**Copyright:** © 2023 by the authors. Licensee MDPI, Basel, Switzerland. This article is an open access article distributed under the terms and conditions of the Creative Commons Attribution (CC BY) license (<https://creativecommons.org/licenses/by/4.0/>).

## 1. Introduction

Deep coal seams have a large amount of gas [1]. Through the excavation of gas extraction roadways [2], arranging coal seam drilling and gas extraction devices in the roadway for gas extraction is widely used in engineering [3–5]. However, due to the complex and changeable deep geological conditions and significant ground stress, it is difficult for conventional support to maintain the stability of the roadway [6–10]. The bolt (cable) can adapt well to bending and shear failure and can also absorb the dynamic load energy in the rock [11–13]. Therefore, it has a great engineering application background for us to select reasonable support parameters for the prestressed bolt (cable) to maintain the stability of the gas extraction roadway [14–16]. Conventional support theories such as the suspension theory, composite beam theory, and surrounding rock reinforcement theory

are no longer applicable [17–19]; the targeted support theory has not yet been formed. The selection of support parameters is often based on experience, and it is difficult to achieve the desired effect [20–22]. Wu, Li et al. [23] proposed to arrange prestressed anchors within a certain range of roadway surrounding rock to form a compression arch to ensure the stability of roadway surrounding rock and the smooth extraction of gas. The numerical simulation method was used to analyze the thickness and strength of the compression arch of prestressed anchors in deep coal and rock, and the reasonable parameters of prestressed anchors were determined. However, the limitation is that only one lithology and prestressed anchor are analyzed, while in practical engineering, it is often multiple lithology [24,25], and prestressed anchor cables are applied to increase the thickness and strength of the compression arch. Based on the analysis of the influence of different lithology and different bolt parameters on the thickness and strength of the compression arch [26,27], this paper further analyzes the influence of the prestressed anchor cable on the thickness and strength of the compression arch and provides a theoretical basis for the determination of reasonable bolt (cable) parameters in the gas extraction roadway.

## 2. Determination of Mechanical Parameters

By taking cores from different parts of the site, a total of three groups with four specimens in each group, the specimens were processed into standard specimens with a diameter of  $d = 50$  mm and a height of  $H = 100$  mm. The laboratory tests the internal friction angle, cohesive force, Poisson's ratio, elastic modulus and other relevant mechanical parameters of the surrounding rock of the roadway. Compress the standard coal and rock specimen with an MTS press and then measure the maximum principal plastic strain and minimum principal plastic strain at different unloading positions after the peak of rock strength. The cohesion ( $c$ ) and internal friction angle ( $\varphi$ ) of the surrounding rock after different lithology peaks are calculated by Formulas (1) and (2).

$$c = \bar{c} + k_1 e^{\frac{-\varepsilon^{ps}}{k_2}} \quad (1)$$

$$\varphi = \bar{\varphi} + k_3 e^{\frac{-\varepsilon^{ps}}{k_4}} \quad (2)$$

where  $\bar{c}$  is the residual bond strength;  $\bar{\varphi}$  is the residual internal friction angle;  $k_1$ ,  $k_2$ ,  $k_3$ , and  $k_4$  are the correlation coefficients; and  $\varepsilon^{ps}$  is the plastic coefficient.

The elastic modulus ( $E$ ) and Poisson's ratio ( $\nu$ ) of coal rock were measured with a rock triaxial shear composite testing machine, and the bulk modulus and shear modulus of surrounding rock were calculated by Formulas (3) and (4).

$$K = E/3(1 - 2\nu) \quad (3)$$

$$G = E/2(1 + \nu) \quad (4)$$

where  $K$  is the bulk modulus of the surrounding rock,  $G$  is the shear modulus of the surrounding rock,  $E$  is the elastic modulus of the surrounding rock measured in the laboratory, and  $\nu$  is the Poisson's ratio of the surrounding rock measured in the laboratory.

The mechanical parameters of the surrounding rock are shown in Table 1.

**Table 1.** Mechanical parameters of surrounding rock.

Lithology	Cohesion, $c$ (MPa)	Internal Friction Angle, $\varphi$ (°)	Bulk Modulus, $K$ (GPa)	Shear Modulus, $G$ (GPa)	Poisson's Ratio, $\nu$
Fractured Mudstone	0.7	18	1.42	0.35	0.36
Mudstone	1.0	22	1.44	0.38	0.35
Sandy Mudstone	1.5	28	1.47	0.45	0.33
Muddy Sandstone	2.0	32	1.50	0.56	0.30

### 3. Numerical Model Building

Combined with the engineering practice of deep roadway in the Huainan and Huaibei mining area of Anhui Province, taking the common straight-wall semi-circular arch roadway in the project as an example, FLAC<sup>3D</sup> software was used for numerical simulation. The roadway section size was taken as the roadway width  $\times$  straight wall height = 4.8 m  $\times$  1.4 m. The strain-softening model was used as the constitutive model, and the Mohr–Coulomb criterion was selected as the yield criterion. The zone gridpoint fix command was used to impose constraints on the bottom and both sides of the model to limit the displacement. The calculation model is shown in Figure 1. The original mesh model radial cylinder and radial tunnel were selected, and the ratio parameter was set to 1.1. The influence range after the excavation of the roadway is generally 5–6 times the radius of the roadway. Therefore, the plane size of the mesh model is length  $\times$  width = 60 m  $\times$  60 m, and the mesh model is shown in Figure 2. The lithology of surrounding rock is fractured mudstone, mudstone, sandy mudstone and muddy sandstone. Change the bolt pre-tightening force to  $F = 50$  kN, 70 kN and 100 kN; the bolt spacing to  $a \times b = 400$  mm  $\times$  400 mm, 500 mm  $\times$  500 mm and 600 mm  $\times$  600 mm; and the bolt length to  $L = 1500$  mm, 2000 mm, 2600 mm and 3000 mm. Then, analyze the typical position of different lithology surrounding rock side and the distribution of additional compressive stress field on the surface of side, and further analyze the influence of prestressed anchor (cable) on the thickness and strength of the compression arch.

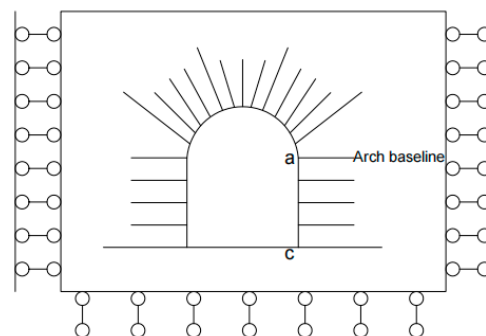


Figure 1. Calculation model.

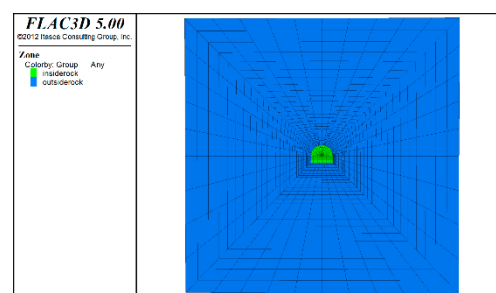


Figure 2. Mesh model.

### 4. Calculation Results and Analysis

#### 4.1. The Influence of Different Bolt Pre-Tightening Forces on the Additional Stress Distribution of Surrounding Rock

Combined with the engineering practice of the Anhui Lianghuai mining area and the tensile strength of the pre-tightening bolt, the pre-tightening force of  $F = 50$  kN, 70 kN and 100 kN can ensure the normal function of the prestressed bolt.

For the supporting conditions of a bolt pre-tightening force of  $F = 50$  kN, bolt spacing of  $a \times b = 400$  mm  $\times$  400 mm and bolt length of  $L = 1.5$  m, the additional stress distribution curves of the surrounding rock at typical positions and surfaces of different lithologies are shown in Figures 3 and 4.

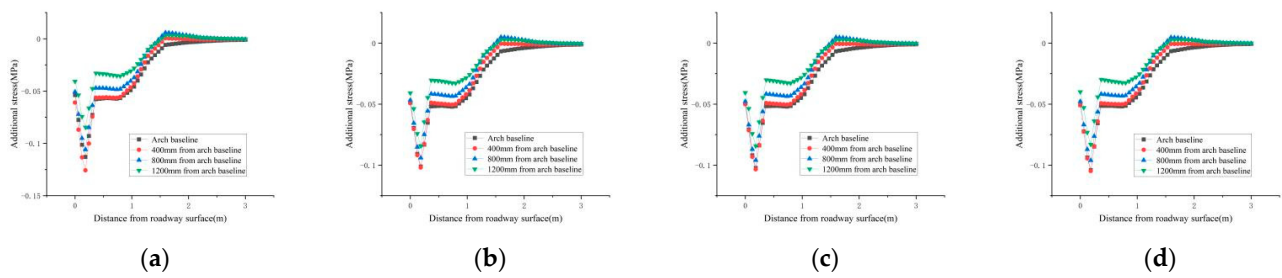


**Figure 3.**  $F = 50$  kN,  $a \times b = 400$  mm  $\times$  400 mm and  $L = 1.5$  m. Distribution diagram of additional stress in surrounding rock. (a) Typical location of fractured mudstone. (b) Typical location of mudstone. (c) Typical location of sandy mudstone. (d) Typical location of muddy sandstone.

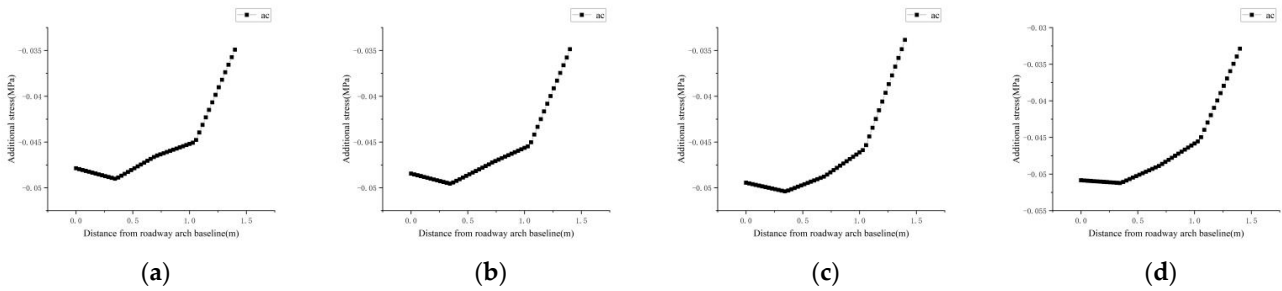


**Figure 4.**  $F = 50$  kN,  $a \times b = 400$  mm  $\times$  400 mm and  $L = 1.5$  m. Distribution diagram of additional stress in surrounding rock. (a) Roadway surface of fractured mudstone. (b) Roadway surface of mudstone. (c) Roadway surface of sandy mudstone. (d) Roadway surface of muddy sandstone.

For the supporting conditions of a bolt pre-tightening force of  $F = 70$  kN, bolt spacing of  $a \times b = 400$  mm  $\times$  400 mm and bolt length of  $L = 1.5$  m, the additional stress distribution curves of the surrounding rock at typical positions and surfaces of different lithologies are shown in Figures 5 and 6.

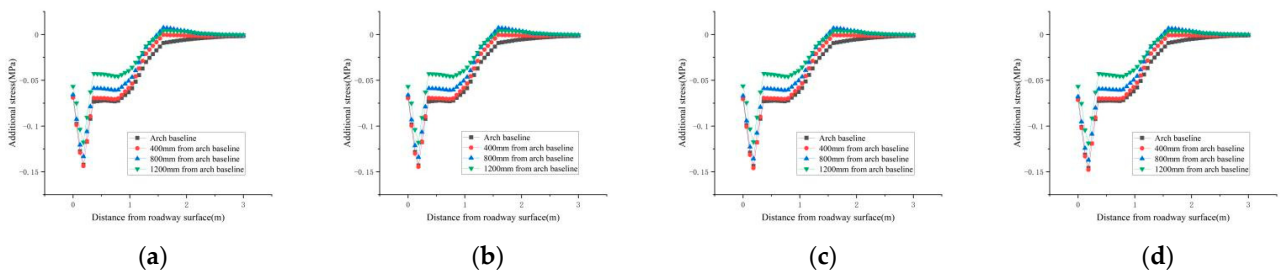


**Figure 5.**  $F = 70$  kN,  $a \times b = 400$  mm  $\times$  400 mm and  $L = 1.5$  m. Distribution diagram of additional stress in surrounding rock. (a) Typical location of fractured mudstone. (b) Typical location of mudstone. (c) Typical location of sandy mudstone. (d) Typical location of muddy sandstone.

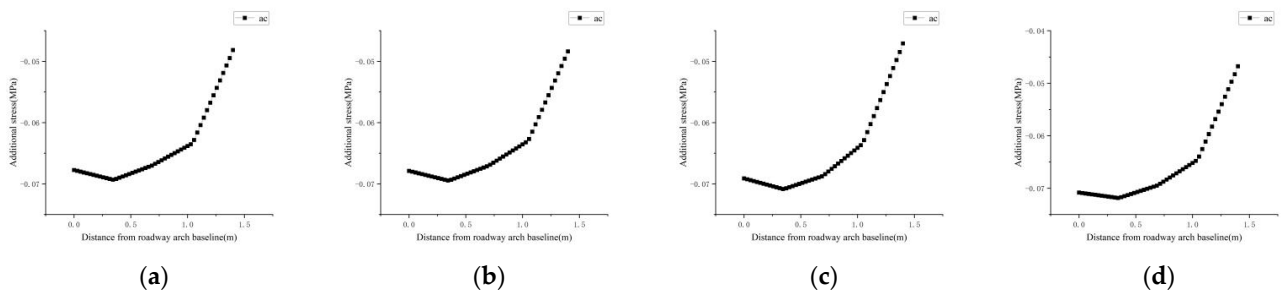


**Figure 6.**  $F = 70$  kN,  $a \times b = 400$  mm  $\times$  400 mm and  $L = 1.5$  m. Distribution diagram of additional stress in surrounding rock. (a) Roadway surface of fractured mudstone. (b) Roadway surface of mudstone. (c) Roadway surface of sandy mudstone. (d) Roadway surface of muddy sandstone.

For the supporting conditions of a bolt pre-tightening force of  $F = 100$  kN, bolt spacing of  $a \times b = 400$  mm  $\times$  400 mm and bolt length of  $L = 1.5$  m, the additional stress distribution curves of the surrounding rock at typical positions and surfaces of different lithologies are shown in Figures 7 and 8.

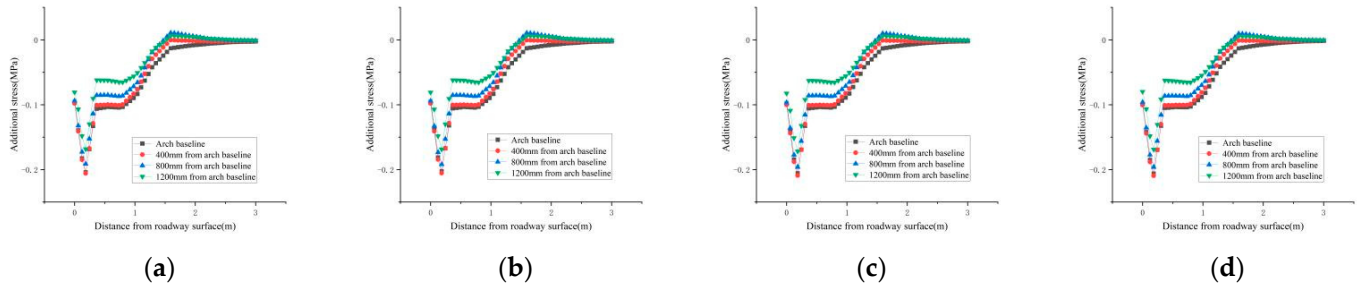


**Figure 7.**  $F = 100$  kN,  $a \times b = 400$  mm  $\times$  400 mm and  $L = 1.5$  m. Distribution diagram of additional stress in surrounding rock. (a) Typical location of fractured mudstone. (b) Typical location of mudstone. (c) Typical location of sandy mudstone. (d) Typical location of muddy sandstone.

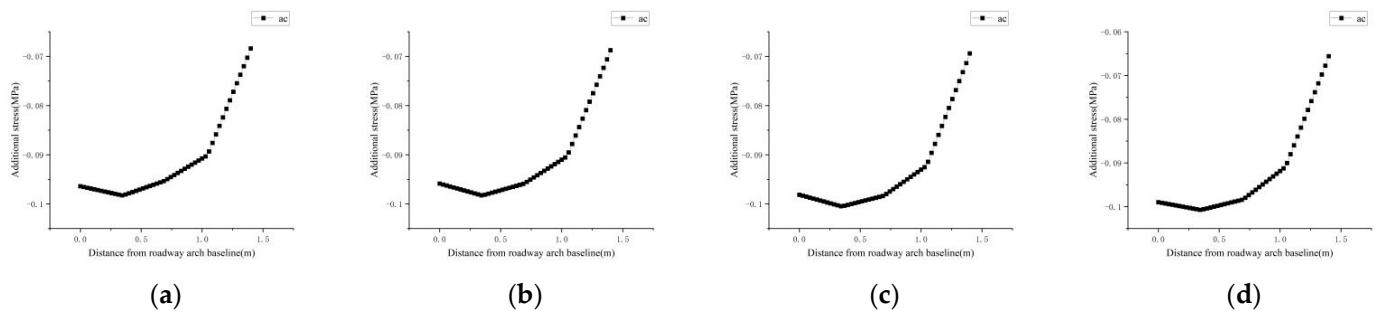


**Figure 8.**  $F = 100$  kN,  $a \times b = 400$  mm  $\times$  400 mm and  $L = 1.5$  m. Distribution diagram of additional stress in surrounding rock. (a) Roadway surface of fractured mudstone. (b) Roadway surface of mudstone. (c) Roadway surface of sandy mudstone. (d) Roadway surface of muddy sandstone.

The above results show the following:

- (1) When the bolt pre-tightening force increases from 50 kN to 100 kN, the additional stress of the surrounding rock fluctuates within a certain range of the roadway surface. As the surface distance of the roadway side increases, the additional stress decreases rapidly.
- (2) The additional stress on the surface of the roadway side increases with the increase of the bolt pre-tightening force, and the additional stress distribution of different lithologies is not obvious. when the bolt pre-tightening force increases from 50 kN to 100 kN, the additional stress of fractured mudstone, mudstone, sandy mudstone and muddy sandstone increases from the ranges 0.05–0.06 MPa, 0.048–0.049 MPa, 0.049–0.05 MPa and 0.0508–0.051 MPa to the ranges 0.094–0.098 MPa, 0.095–0.098 MPa, 0.098–0.10 MPa and 0.099–0.10 MPa, respectively. The lithology of sandy mudstone and muddy sandstone is better, and the fluctuation range of additional stress on the surface of the side is smaller.
- (3) The additional stress at the typical position of the roadway side increases with the increase of the bolt pre-tightening force. When the bolt pre-tightening force of  $F = 50$  kN increased to 100 kN, the average additional stress of fractured mudstone, mudstone, sandy mudstone and muddy sandstone increased from 0.062 MPa, 0.062 MPa, 0.062 MPa and 0.062 MPa to 0.12 MPa, 0.12 MPa, 0.12 MPa and 0.12 MPa, respectively. The additional stress at the place where the roadway side is close to the arch baseline is large.

#### 4.2. The Influence of Different Bolt Length on the Additional Stress Distribution of Surrounding Rock

For the supporting conditions of a bolt pre-tightening force of  $F = 100$  kN, bolt spacing of  $a \times b = 400$  mm  $\times$  400 mm and bolt length of  $L = 2.0$  m, the additional stress distribution curves of surrounding rock at typical positions and surfaces of different lithologies are shown in Figures 9 and 10.

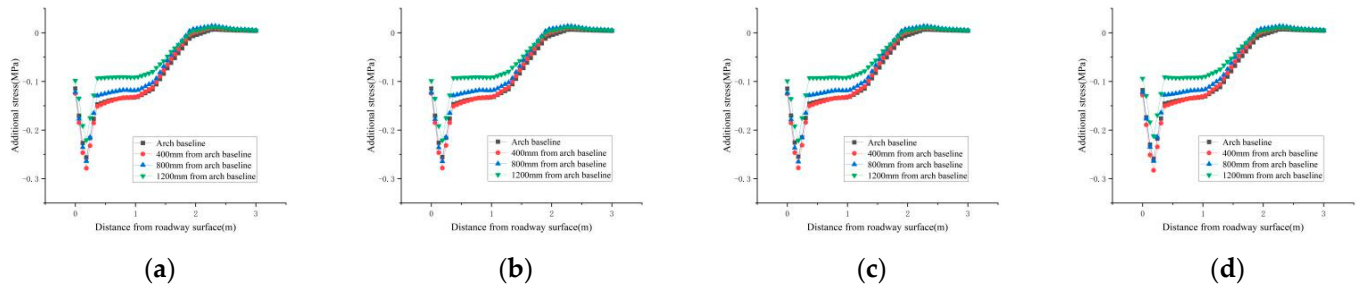


**Figure 9.**  $F = 100$  kN,  $a \times b = 400$  mm  $\times$  400 mm and  $L = 2.0$  m. Distribution diagram of additional stress in surrounding rock. (a) Typical location of fractured mudstone. (b) Typical location of mudstone. (c) Typical location of sandy mudstone. (d) Typical location of muddy sandstone.

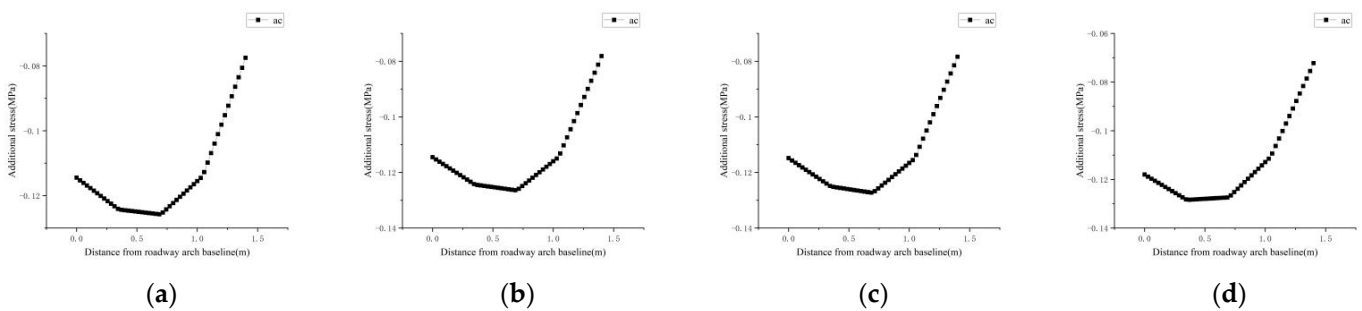


**Figure 10.**  $F = 100$  kN,  $a \times b = 400$  mm  $\times$  400 mm and  $L = 2.0$  m. Distribution diagram of additional stress in surrounding rock. (a) Roadway surface of fractured mudstone. (b) Roadway surface of mudstone. (c) Roadway surface of sandy mudstone. (d) Roadway surface of muddy sandstone.

For the supporting conditions of a bolt pre-tightening force of  $F = 100$  kN, bolt spacing of  $a \times b = 400$  mm  $\times$  400 mm and bolt length of  $L = 2.6$  m, the additional stress distribution curves of the surrounding rock at typical positions and surfaces of different lithologies are shown in Figures 11 and 12.

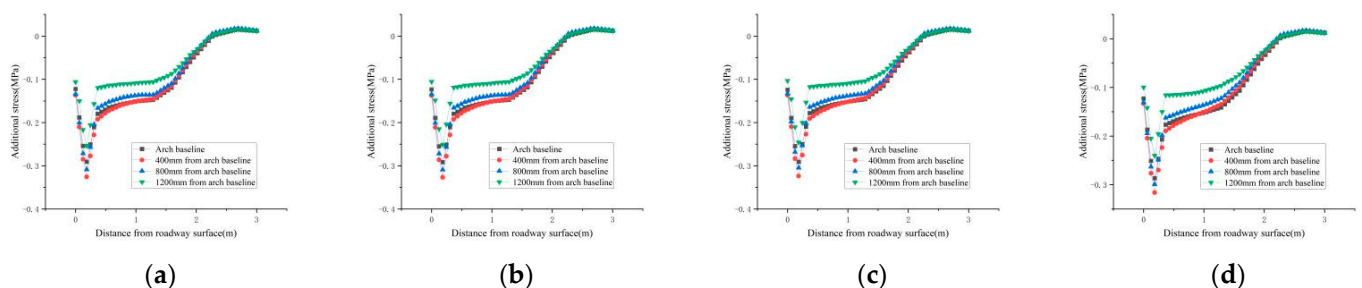


**Figure 11.**  $F = 100$  kN,  $a \times b = 400$  mm  $\times$  400 mm and  $L = 2.6$  m. Distribution diagram of additional stress in surrounding rock. (a) Typical location of fractured mudstone. (b) Typical location of mudstone. (c) Typical location of sandy mudstone. (d) Typical location of muddy sandstone.

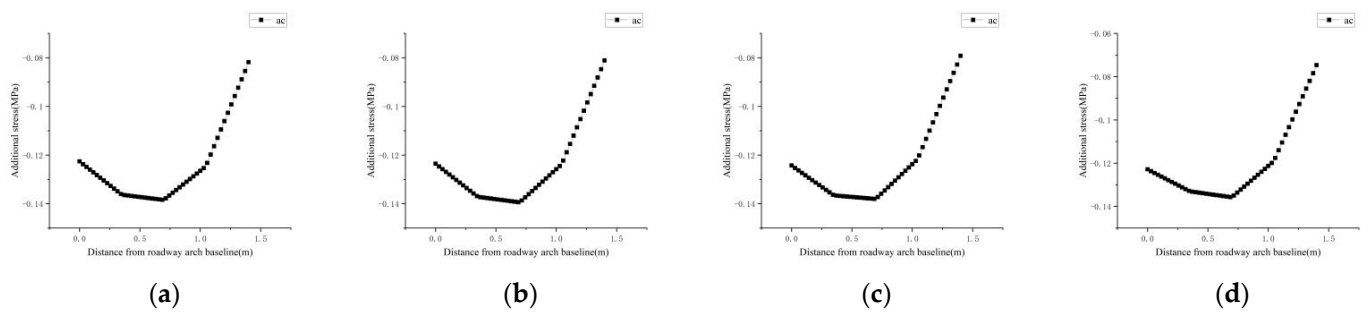


**Figure 12.**  $F = 100$  kN,  $a \times b = 400$  mm  $\times$  400 mm and  $L = 2.6$  m. Distribution diagram of additional stress in surrounding rock. (a) Roadway surface of fractured mudstone. (b) Roadway surface of mudstone. (c) Roadway surface of sandy mudstone. (d) Roadway surface of muddy sandstone.

For the supporting conditions of a bolt pre-tightening force of  $F = 100$  kN, bolt spacing of  $a \times b = 400$  mm  $\times$  400 mm and bolt length of  $L = 3.0$  m, the additional stress distribution curves of the surrounding rock at typical positions and surfaces of different lithologies are shown in Figures 13 and 14.

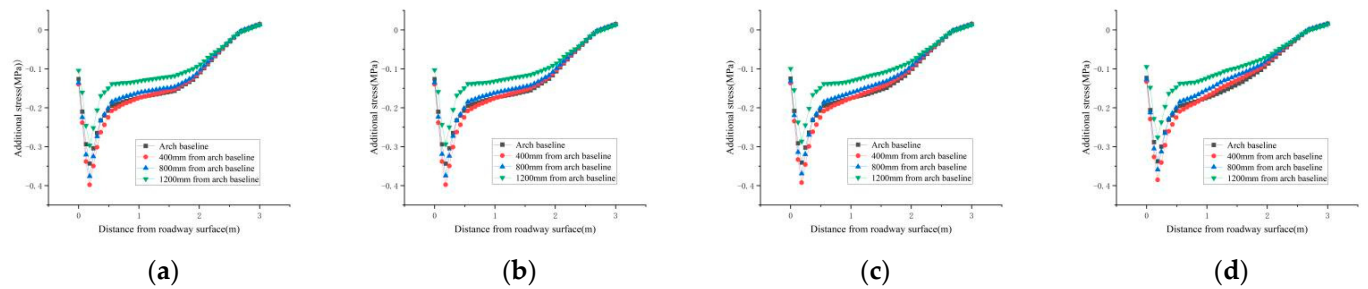


**Figure 13.**  $F = 100$  kN,  $a \times b = 400$  mm  $\times$  400 mm and  $L = 3.0$  m. Distribution diagram of additional stress in surrounding rock. (a) Typical location of fractured mudstone. (b) Typical location of mudstone. (c) Typical location of sandy mudstone. (d) Typical location of muddy sandstone.

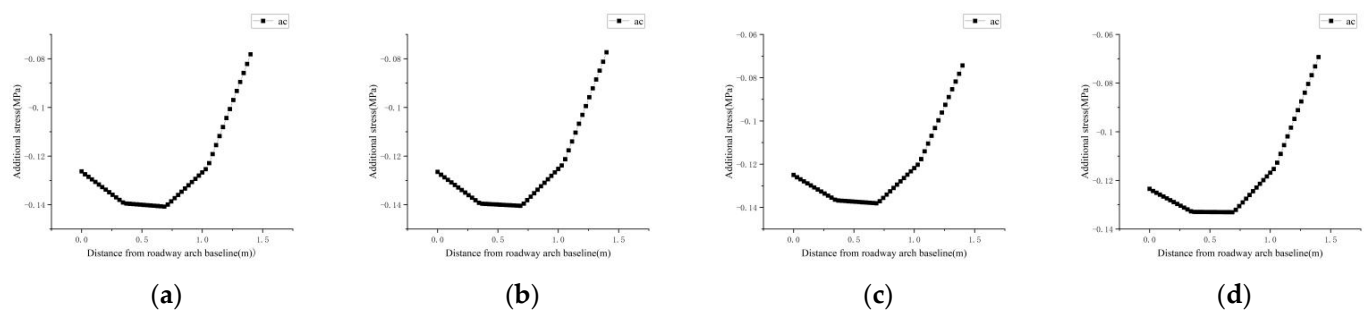


**Figure 14.**  $F = 100$  kN,  $a \times b = 400$  mm  $\times$  400 mm and  $L = 3.0$  m. Distribution diagram of additional stress in surrounding rock. (a) Roadway surface of fractured mudstone. (b) Roadway surface of mudstone. (c) Roadway surface of sandy mudstone. (d) Roadway surface of muddy sandstone.

The above results show the following:

- (1) When the bolt length increases from 1.5 m to 3.0 m, the additional stress of the surrounding rock fluctuates within a certain range of the roadway surface. As the surface distance of the roadway side increases, the additional stress decreases rapidly.
- (2) The additional stress on the surface of the roadway side increases with the increase of the bolt length, and the additional stress distribution of different lithologies is not obvious. When the length of the bolt increases from 1.5 m to 3.0 m, the additional stress of the fractured mudstone, mudstone, sandy mudstone and muddy sandstone increases from the ranges of 0.096–0.101 MPa, 0.096–0.100 MPa, 0.098–0.101 MPa and 0.099–0.101 MPa to the ranges of 0.126–0.141 MPa, 0.127–0.141 MPa, 0.128–0.140 MPa

and 0.139–0.140 MPa, respectively. The lithology of sandy mudstone and muddy sandstone is better, and the fluctuation range of additional stress on the surface of the side is smaller.

- (3) The additional stress at the typical position of the roadway side decreases with the increase of the bolt spacing. When the bolt spacing ( $a \times b$ ) increases from  $400 \text{ mm} \times 400 \text{ mm}$  to  $600 \text{ mm} \times 600 \text{ mm}$ , the average additional stress of fractured mudstone, mudstone, sandy mudstone and muddy sandstone decreases from 0.17 MPa, 0.17 MPa, 0.17 MPa and 0.17 MPa to 0.14 MPa, 0.14 MPa, 0.14 MPa and 0.14 MPa, respectively. The additional stress at the place where the roadway side is close to the arch baseline is large.

#### 4.3. The Influence of Different Bolt Spacing on the Additional Stress Distribution of Surrounding Rock

For the supporting conditions of a bolt pre-tightening force of  $F = 100 \text{ kN}$ , bolt spacing of  $a \times b = 500 \text{ mm} \times 500 \text{ mm}$  and bolt length of  $L = 2.6 \text{ m}$ , the additional stress distribution curves of the surrounding rock at typical positions and surfaces of different lithologies are shown in Figures 15 and 16.

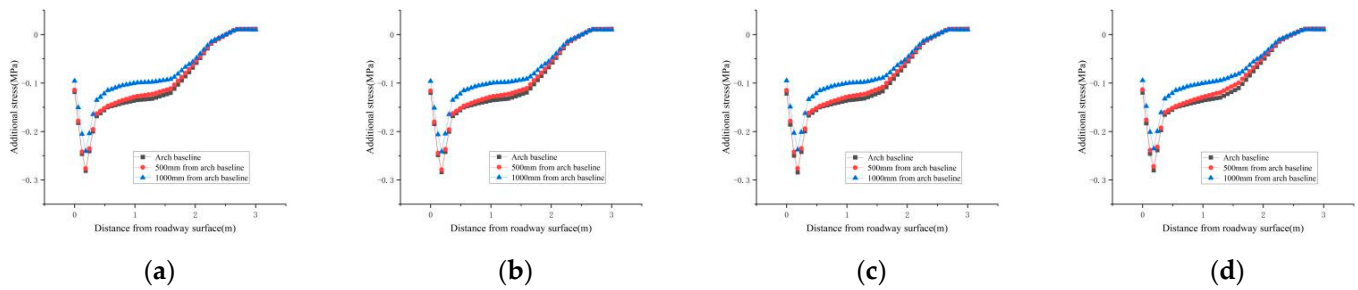


**Figure 15.**  $F = 100 \text{ kN}$ ,  $a \times b = 500 \text{ mm} \times 500 \text{ mm}$  and  $L = 2.6 \text{ m}$ . Distribution diagram of additional stress in surrounding rock. (a) Typical location of fractured mudstone. (b) Typical location of mudstone. (c) Typical location of sandy mudstone. (d) Typical location of muddy sandstone.

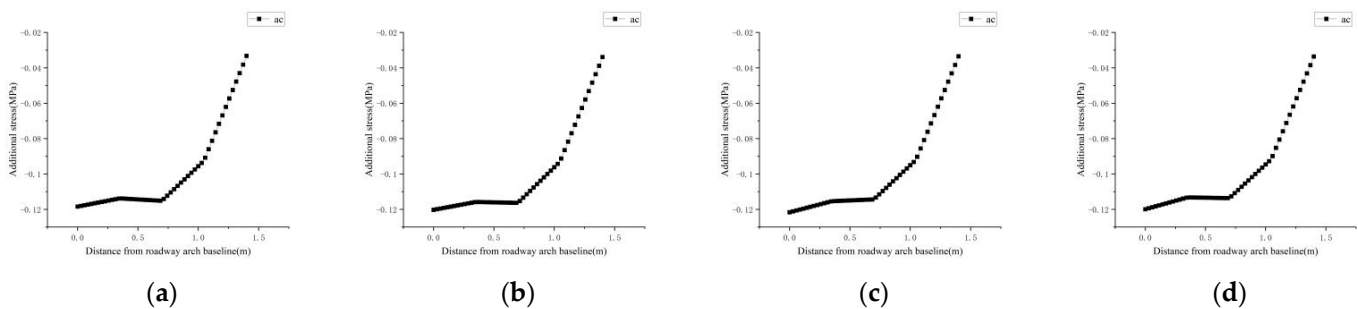


**Figure 16.**  $F = 100 \text{ kN}$ ,  $a \times b = 500 \text{ mm} \times 500 \text{ mm}$  and  $L = 2.6 \text{ m}$ . Distribution diagram of additional stress in surrounding rock. (a) Roadway surface of fractured mudstone. (b) Roadway surface of mudstone. (c) Roadway surface of sandy mudstone. (d) Roadway surface of muddy sandstone.

For the supporting conditions of a bolt pre-tightening force of  $F = 100 \text{ kN}$ , bolt spacing of  $a \times b = 600 \text{ mm} \times 600 \text{ mm}$  and bolt length of  $L = 2.6 \text{ m}$ , the additional stress distribution curves of the surrounding rock at typical positions and surfaces of different lithologies are shown in Figures 17 and 18.

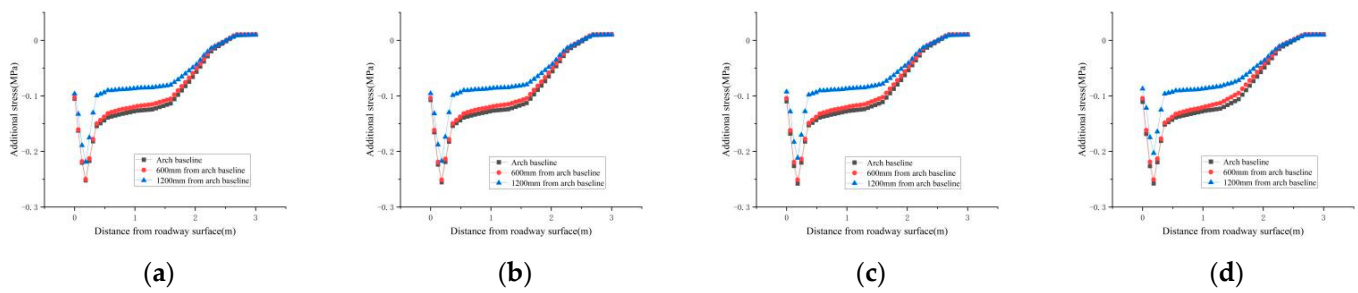


**Figure 17.**  $F = 100$  kN,  $a \times b = 600$  mm  $\times$  600 mm and  $L = 2.6$  m. Distribution diagram of additional stress in surrounding rock. (a) Typical location of fractured mudstone. (b) Typical location of mudstone. (c) Typical location of sandy mudstone. (d) Typical location of muddy sandstone.

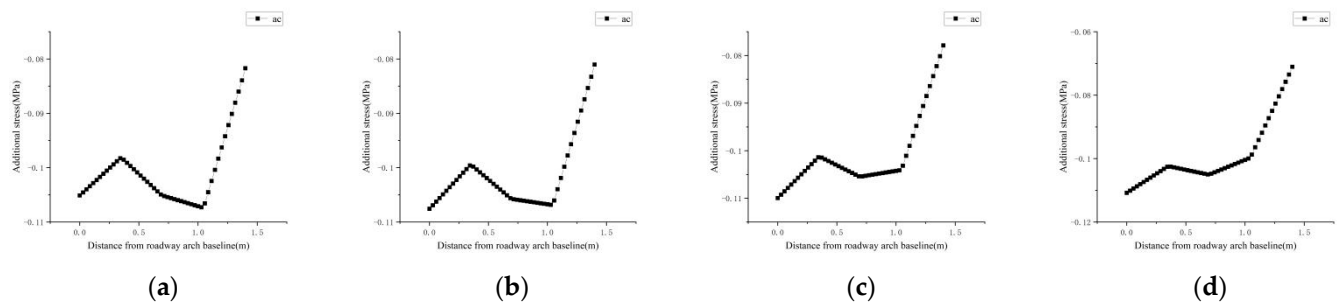


**Figure 18.**  $F = 100$  kN,  $a \times b = 600$  mm  $\times$  600 mm and  $L = 2.6$  m. Distribution diagram of additional stress in surrounding rock. (a) Roadway surface of fractured mudstone. (b) Roadway surface of mudstone. (c) Roadway surface of sandy mudstone. (d) Roadway surface of muddy sandstone.

The above results show the following:

- (1) When the bolt row spacing increases from 400 mm  $\times$  400 mm to 600 mm  $\times$  600 mm, the additional stress of the surrounding rock fluctuates within a certain range of the roadway surface. As the surface distance of the roadway side increases, the additional stress decreases rapidly.
- (2) The additional stress on the surface of the roadway side decreases with the increase of the bolt spacing, and the additional stress distribution of different lithologies is not obvious. When the bolt row spacing increases from 400 mm  $\times$  400 mm to 600 mm  $\times$  600 mm, the additional stress of the fractured mudstone, mudstone, sandy mudstone and muddy sandstone decreases from the ranges of 0.128–0.138 MPa, 0.124–0.139 MPa, 0.124–0.138 MPa and 0.123–0.136 MPa to the ranges of 0.098–0.105 MPa, 0.099–0.105 MPa, 0.099–0.104 MPa and 0.100–0.103 MPa, respectively. The lithology of sandy mudstone and muddy sandstone is better, and the fluctuation range of additional stress on the surface of the side is smaller.
- (3) When the bolt row spacing is  $a \times b = 400$  mm  $\times$  400 mm, the average additional stress of fractured mudstone, mudstone, sandy mudstone and muddy sandstone is 0.17 MPa, 0.17 MPa, 0.17 MPa and 0.17 MPa. When the bolt row spacing is  $a \times b = 600$  mm  $\times$  600 mm, the average additional stress is 0.14 MPa, 0.14 MPa, 0.14 MPa and 0.14 MPa. The additional stress at the place where the roadway side is close to the arch baseline is large.

#### 4.4. Calculation of Compression Arch Thickness of Prestressed Anchors under Different Lithologies

The additional stress field compression arch formed by the bolt and anchor cable with a certain pre-tightening force has the following characteristics: The pre-tightening force of the bolt and anchor cable is usually expressed in a cone shape, which extends from the end of the prestressed bolt and anchor cable and distributes itself to the inside of the rock around the roadway. Under the reasonable row spacing, the additional stress field formed by the prestressed anchor and anchor cable begins to superimpose at the end of the anchor

and anchor cable, forming a compression arch with a certain thickness. The additional stress formed near the end of the anchor and anchor cable is the largest.

The relationship between the thickness of the compression arch of the bolt (cable) and the length and spacing of the bolt (cable) is shown in (5).

$$m = L_1 - \frac{a}{2\alpha} \quad (5)$$

where  $m$  is the thickness of compression arch,  $L_1$  is the effective length of prestressed anchor (cable),  $a$  is the row spacing and  $\alpha$  is the angle of the prestressed anchor (cable).

The arch thickness of the compression arch is shown in Table 2 for the support of only bolts.

**Table 2.** The thickness of the compression arch formed only under bolt support.

Bolt Support Parameters	Fractured Mudstone (m)	Mudstone (m)	Sandy Mudstone (m)	Muddy Sandstone (m)
F = 50 kN, a × b = 400 mm × 400 mm and L = 1.5 m	0.73	0.73	0.73	0.73
F = 70 kN, a × b = 400 mm × 400 mm and L = 1.5 m	0.80	0.80	0.80	0.80
F = 100 kN, a × b = 400 mm × 400 mm and L = 1.5 m	0.85	0.85	0.85	0.85
F = 100 kN, a × b = 400 mm × 400 mm and L = 2.0 m	1.22	1.22	1.22	1.22
F = 100 kN, a × b = 400 mm × 400 mm and L = 2.6 m	1.60	1.60	1.60	1.60
F = 100 kN and a × b = 400 mm × 400 mm and L = 3.0 m	1.84	1.84	1.84	1.84
F = 100 kN, a × b = 500 mm × 500 mm and L = 2.6 m	1.59	1.59	1.59	1.59
F = 100 kN, a × b = 600 mm × 600 mm and L = 2.6 m	1.59	1.59	1.59	1.59

Table 3 shows the arch thickness of the compression under the supporting conditions of bolt parameters F = 100 kN, a × b = 400 × 400 mm and L = 3.0 m after changing the supporting parameters of the anchor cable.

**Table 3.** The thickness of the compression arch formed by adding an anchor cable.

Anchor Cable Support Parameters	Fractured Mudstone (m)	Mudstone (m)	Sandy Mudstone (m)	Muddy Sandstone (m)
F = 80 kN, a × b = 400 mm × 400 mm and L = 3.0 m	1.83	1.85	1.83	1.86
F = 100 kN, a × b = 400 mm × 400 mm and L = 3.0 m	1.87	1.87	1.89	1.86
F = 120 kN, a × b = 400 mm × 400 mm and L = 3.0 m	1.88	1.89	1.89	1.87
F = 100 kN, a × b = 400 mm × 400 mm and L = 4.0 m	1.88	1.89	1.88	1.87
F = 100 kN, a × b = 400 mm × 400 mm and L = 6.0 m	1.86	1.87	1.88	1.88

The above results show the following:

- (1) When the bolt spacing is a × b = 400 mm × 400 mm, and the bolt length is L = 1.5 m, by changing the size of the bolt pre-tightening force, when the pre-tightening force (F) increases from 50 kN to 100 kN, the thickness of the compression arch formed by the four lithologies increases from 0.73 m to 0.85 m, which is a small increase.
- (2) When the bolt pre-tightening force is F = 100 kN, and the bolt spacing is a × b = 400 mm × 400 mm, by changing the bolt length, when the bolt length (L) increases from 1.5 m to 3.0 m, the thickness of the compression arch formed by the four lithologies increases from 0.85 m to 1.84 m. Compared with changing the bolt pre-tightening force, changing the bolt length has a better effect on increasing the thickness of the compression arch.
- (3) By changing the bolt spacing, the anchor cable pre-tightening force and the anchor cable length, the changes in the thickness of the compression arch formed by the four lithologies is not obvious.

#### 4.5. Calculation of Compression Arch Strength of Prestressed Anchors under Different Lithologies

After installing high-strength prestressed bolts in the deep soft surrounding rock roadway, a triangular stress field will be formed around the head and end of bolts under the pre-tightening anchoring agent and tray. Through the role of the stress field at both ends, the mechanical properties of the rock layer are improved, and its bearing capacity is improved. In the process of roadway excavation, the parameters of bolt (cable) are reasonably selected, and the pre-tightening force is applied to make the rock of roadway form a compression arch with high bearing capacity to maintain the stability of the roadway.

The increased strength of the compression arch is calculated by Formula (6).

$$\Delta\sigma = 2c \frac{\cos\varphi}{1 - \sin\varphi} \quad (6)$$

According to the change of cohesion and internal friction angle of surrounding rock, the percentage of different bolt (cable) support parameters to improve the strength of surrounding rock compression arch is obtained. The calculation results are shown in Tables 4–7 only under the bolt support, and the calculation results are shown in Tables 8 and 9 under the joint support of the bolt and the anchor cable.

##### 4.5.1. The Percentage Increase of Compressive Arch Strength of Roadway Surrounding Rock Only under Bolt Support

###### (1) At the arch baseline position

**Table 4.** The percentage increase in the strength of the compression arch of roadway surrounding rock at the arch baseline location under bolt support.

Bolt Support Parameters	Fractured Mudstone	Mudstone	Sandy Mudstone	Muddy Sandstone
F = 50 kN, a × b = 400 mm × 400 mm and L = 1.5 m	7%	4%	3%	3%
F = 70 kN, a × b = 400 mm × 400 mm and L = 1.5 m	9%	7%	5%	4%
F = 100 kN, a × b = 400 mm × 400 mm and L = 1.5 m	12%	9%	7%	5%
F = 100 kN, a × b = 400 mm × 400 mm and L = 2.0 m	15%	11%	8%	7%
F = 100 kN, a × b = 400 mm × 400 mm and L = 2.6 m	17%	13%	9%	8%
F = 100 kN, a × b = 400 mm × 400 mm and L = 3.0 m	20%	15%	11%	9%
F = 100 kN, a × b = 500 mm × 500 mm and L = 2.6 m	16%	12%	9%	7%
F = 100 kN, a × b = 600 mm × 600 mm and L = 2.6 m	14%	10%	8%	6%

###### (2) At 400 mm from the arch baseline location

**Table 5.** The percentage increase in the strength of the compression arch of roadway surrounding rock at 400 mm from the arch baseline location under bolt support.

Bolt Support Parameters	Fractured Mudstone	Mudstone	Sandy Mudstone	Muddy Sandstone
F = 50 kN, a × b = 400 mm × 400 mm and L = 1.5 m	7%	5%	4%	3%
F = 70 kN, a × b = 400 mm × 400 mm and L = 1.5 m	9%	6%	5%	4%
F = 100 kN, a × b = 400 mm × 400 mm and L = 1.5 m	12%	9%	7%	5%
F = 100 kN, a × b = 400 mm × 400 mm and L = 2.0 m	15%	11%	8%	7%
F = 100 kN, a × b = 400 mm × 400 mm and L = 2.6 m	17%	13%	9%	8%
F = 100 kN, a × b = 400 mm × 400 mm and L = 3.0 m	20%	15%	11%	9%

###### (3) At 800 mm from the arch baseline location

**Table 6.** The percentage increase in the strength of the compression arch of roadway surrounding rock at 800 mm from the arch baseline location under bolt support.

Bolt Support Parameters	Fractured Mudstone	Mudstone	Sandy Mudstone	Muddy Sandstone
F = 50 kN, a × b = 400 mm × 400 mm and L = 1.5 m	6%	5%	3%	3%
F = 70 kN, a × b = 400 mm × 400 mm and L = 1.5 m	8%	6%	4%	3%
F = 100 kN, a × b = 400 mm × 400 mm and L = 1.5 m	11%	8%	6%	4%
F = 100 kN, a × b = 400 mm × 400 mm and L = 2.0 m	14%	10%	7%	6%
F = 100 kN, a × b = 400 mm × 400 mm and L = 2.6 m	16%	12%	8%	7%
F = 100 kN, a × b = 400 mm × 400 mm and L = 3.0 m	19%	14%	10%	8%

(4) At 1200 mm from the arch baseline location

**Table 7.** The percentage increase in the strength of the compression arch of roadway surrounding rock at 1200 mm from the arch baseline location under bolt support.

Bolt Support Parameters	Fractured Mudstone	Mudstone	Sandy Mudstone	Muddy Sandstone
F = 50 kN, a × b = 400 mm × 400 mm and L = 1.5 m	5%	4%	2%	2%
F = 70 kN, a × b = 400 mm × 400 mm and L = 1.5 m	6%	5%	3%	2%
F = 100 kN, a × b = 400 mm × 400 mm and L = 1.5 m	8%	6%	5%	4%
F = 100 kN, a × b = 400 mm × 400 mm and L = 2.0 m	11%	8%	6%	5%
F = 100 kN, a × b = 400 mm × 400 mm and L = 2.6 m	12%	9%	7%	5%
F = 100 kN, a × b = 400 mm × 400 mm and L = 3.0 m	15%	11%	8%	7%

The above results show the following:

- (1) Under different bolt parameters' support, the percentage increase of the strength of the compression arch formed by sandy mudstone is between 3 and 11%, and the percentage increase of the strength of the compression arch formed by muddy sandstone is between 3 and 9%, which was a small increase; the percentage increase of the strength of the compression arch formed by fractured mudstone is between 7 and 20%, and the percentage increase of strength of the compression arch formed by mudstone is between 4 and 15%, so the increase is more obvious.
- (2) When the bolt spacing is a × b = 400 mm × 400 mm, and the bolt length is L = 1.5 m, by changing the bolt pre-tightening force, when the bolt pre-tightening force (F) increases from 50 kN to 100 kN, the percentage increase of the strength of the compression arch formed by fractured mudstone, mudstone, sandy mudstone and muddy sandstone increases from 7%, 4%, 3% and 3% to 12%, 9%, 7% and 5%, which was a small increase.
- (3) When the bolt pre-tightening force is F = 100 kN, and the bolt spacing is a × b = 400 mm × 400 mm, by changing the bolt length, when the bolt length (L) increases from 1.5 m to 3.0 m, the percentage increase of the strength of the compression arch formed by fractured mudstone, mudstone, sandy mudstone and muddy sandstone increases from 12%, 9%, 7% and 5% to 20%, 15%, 11% and 9%, which was a large increase.
- (4) Under the same bolt parameters support, the increase of the strength of the compression arch at different positions of the same roadway side is different. The closer to the arch baseline, the more obvious the increase.

4.5.2. The Percentage Increase of Compressive Arch Strength of Roadway Surrounding Rock by Adding Different Anchor Cable Parameters when the Bolt Parameters Are F = 100 kN, a × b = 400 mm × 400 mm and L = 3.0 m

- (1) At 400 mm from the arch baseline location

**Table 8.** The percentage increase in the strength of the compression arch of roadway surrounding rock at 400 mm from the arch baseline location under bolt and cable support.

Anchor Cable Support Parameters	Fractured Mudstone	Mudstone	Sandy Mudstone	Muddy Sandstone
F = 80 kN, a × b = 400 mm × 400 mm, L = 3.0 m	22%	16%	12%	10%
F = 100 kN, a × b = 400 mm × 400 mm, L = 3.0 m	23%	17%	13%	11%
F = 120 kN, a × b = 400 mm × 400 mm, L = 3.0 m	24%	18%	14%	12%
F = 100 kN, a × b = 400 mm × 400 mm, L = 4.0 m	26%	19%	15%	13%
F = 100 kN, a × b = 400 mm × 400 mm, L = 6.0 m	26%	19%	15%	13%

(2) At 800 mm from the arch baseline location

**Table 9.** The percentage increase in the strength of the compression arch of roadway surrounding rock at 800 mm from the arch baseline location under bolt and cable support.

Anchor Cable Support Parameters	Fractured Mudstone	Mudstone	Sandy Mudstone	Muddy Sandstone
F = 80 kN, a × b = 400 mm × 400 mm, L = 3.0 m	25%	19%	14%	11%
F = 100 kN, a × b = 400 mm × 400 mm, L = 3.0 m	27%	20%	15%	12%
F = 120 kN, a × b = 400 mm × 400 mm, L = 3.0 m	28%	21%	16%	13%
F = 100 kN, a × b = 400 mm × 400 mm, L = 4.0 m	31%	23%	17%	14%
F = 100 kN, a × b = 400 mm × 400 mm, L = 6.0 m	32%	24%	18%	14%

The above results show the following:

- (1) When the bolt pre-tightening force is  $F = 100$  kN, the bolt length is  $L = 3.0$  m and the bolt spacing is  $a \times b = 400$  mm  $\times$  400 mm, by adding different anchor cable parameters to bolster the bolt's support, the percentage increase of the strength of the compression arch formed by sandy mudstone is between 12 and 15%, and the percentage increase of the strength of the compression arch formed by muddy sandstone is between 10 and 13%, which is a small increase; the percentage increase of the strength of the compression arch formed by fractured mudstone is between 22 and 26%, and the percentage increase of the strength of the compression arch formed by mudstone is between 16 and 19%, so the increase is more obvious.
- (2) Under the support of the same bolt and anchor cable parameters, the better the lithology, the smaller the percentage increase of the strength of the compression arch; the worse the lithology, the more obvious the percentage increase of the strength of the compression arch.
- (3) By changing the anchor cable pre-tightening force and the anchor cable length, the changes of the strength of the compression arch formed by the four lithologies become more obvious.

## 5. Engineering Verification

### 5.1. Layout of Multi-Point Displacement Meter

In order to further verify the thickness of compression arch, this project used a pinhole multi-point displacement meter to measure the fragmentation and displacement of the roadway surrounding rock, arranged the anchor claw head at the location of the measurement point and extended the displacement meter into the location of the measurement point in the roadway and fixed it. When the surrounding rock deforms with time, it is transmitted to the displacement recording sensor through the wire rope connected to the anchor head, and the corresponding surrounding rock is judged by the amount of change in the length of the wire rope. Multi-point displacement meters are arranged in the direction of the arch baseline of the roadway, and five measuring points, i.e., A, B, C, D and E, are arranged at 0.8 m, 1.8 m, 2.0 m, 4.4 m and 7.5 m from the surface of the roadway, respectively. Because the measuring point E is located in the original rock stress area, there

is almost no deformation, so the displacement of this point can be ignored. By calculating the displacement difference between other anchor claws, the broken state and approximate range of the roadway are estimated. Among them, the KJ327-F intelligent mine-pressure monitoring substation is selected for measurement, and data and records are collected every 2 h. The diagram of the multi-point displacement meter arrangement is shown in Figure 19. The numerical simulation shows that the displacement of the A, B, C, D and E measuring points changes with the distance from the surface of the roadway, as shown in Figure 20. The displacement of the arch baseline position of the roadway side is the same in a certain area (1800 mm), about 130 mm.

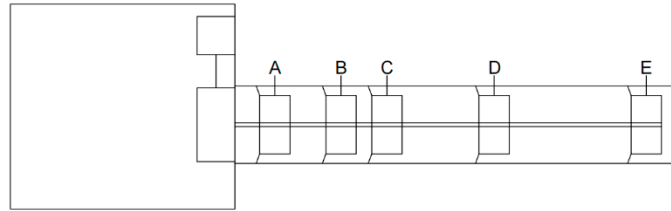


Figure 19. Layout of multi-point displacement meter measuring point.

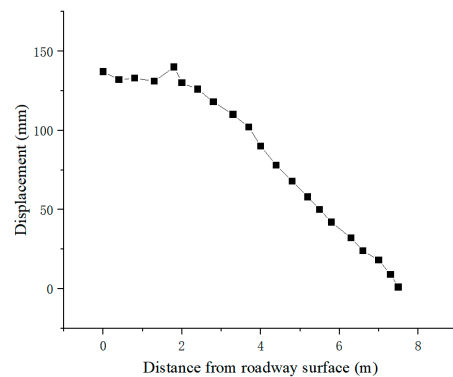


Figure 20. Displacement distribution of roadway surrounding rock.

### 5.2. Field Measurement

Through the data acquisition of the multi-point displacement meter, the displacement of A, B, C, D and E points is analyzed as shown in Table 10.

Table 10. Displacement of each measuring point.

Measuring Point	A	B	C	D	E
Displacement (mm)	133	140	130	78	1

It can be seen from Table 10 that the actual displacement of the roadway is basically consistent with the numerical simulation results, thus verifying the reliability of the numerical simulation.

## 6. Conclusions

The conclusions and main achievements of this paper can be summarized as follows:

- (1) The lithology of surrounding rock and the row spacing between bolts have no significant influence on the thickness of the compression arch, while the length of bolts and pre-tightening force have significant influence on the thickness of the compression arch, and the increase of the compression arch thickness is helpful to improve the stability of the roadway. When the bolt length is  $L = 1.5$  m, bolt spacing is  $a \times b = 400 \text{ mm} \times 400 \text{ mm}$  and bolt pre-tightening force increased from  $F = 50 \text{ kN}$  to  $F = 100 \text{ kN}$ , the thickness of the compression arch formed by the four lithologies

increased by 0.12 m. When the bolt pre-tightening force was  $F = 100$  kN, the bolt spacing was  $a \times b = 400 \text{ mm} \times 400 \text{ mm}$  and the bolt length of  $L = 1.5$  m increased to  $L = 3.0$  m, the thickness of the compression arch formed by the four lithologies increased by 0.99 m. When the bolt pre-tightening force was  $F = 100$  kN, the bolt length was  $L = 2.6$  m and the bolt spacing of  $a \times b = 400 \text{ mm} \times 400 \text{ mm}$  increased to  $a \times b = 500 \text{ mm} \times 500 \text{ mm}$  and  $a \times b = 600 \text{ mm} \times 600 \text{ mm}$ , the thickness of the compression arch formed by the four lithologies was reduced by 0.01 m.

- (2) The influence of the surrounding rock lithology, bolt pre-tightening force, bolt length and row spacing on the strength of the compression arch is significant. At the arch baseline position, when the bolt pre-tightening force increased from  $F = 50$  kN to  $F = 100$  kN, the percentage increase of the compressive arch strength formed by four kinds of lithologies increased from 7%, 4%, 3% and 3% to 12%, 9%, 7% and 5%. When the bolt length increased from  $L = 1.5$  m to  $L = 3.0$  m, the percentage increase of the compressive arch strength formed by four kinds of lithology increased from 12%, 9%, 7% and 5% to 20%, 15%, 11% and 9%. When the bolt spacing increased from  $a \times b = 400 \text{ mm} \times 400 \text{ mm}$  to  $a \times b = 600 \text{ mm} \times 600 \text{ mm}$ , the percentage increase of compressive arch strength formed by four kinds of lithology decreased from 17%, 13%, 9% and 8% to 14%, 10%, 8% and 6%.
- (3) The pre-tightening force and length of the anchor cable have no obvious effect on the thickness of the compression arch but have a significant effect on the strength of the compression arch. On the basis of bolt pre-tightening force being  $F = 100$  kN, bolt length being  $L = 3.0$  m and bolt spacing being  $a \times b = 400 \times 400$  mm, the anchor cable and bolt are added to support together. When the anchor cable pre-tightening force increased from  $F = 80$  kN to  $F = 120$  kN, the thickness of the compression arch formed by four kinds of lithologies increased from 1.83 m, 1.85 m, 1.83 m and 1.86 m to 1.88 m, 1.89 m, 1.89 m and 1.87 m; and the percentage increase of the strength of the compressive arch increased from 22%, 16%, 12% and 10% to 24%, 18%, 14% and 12%. When the anchor cable length increased from  $L = 3.0$  m to  $L = 6.0$  m, the thickness of the compression arch formed by the four kinds of lithologies changed from 1.87 m, 1.87 m, 1.89 m and 1.86 m to 1.86 m, 1.87 m, 1.88 m and 1.88 m; and the percentage increase of the strength of the compression arch increased from 23%, 17%, 13% and 11% to 26%, 19%, 15% and 13%.

**Author Contributions:** Software, N.L. and S.Z.; Validation, D.W.; Investigation, N.L. and S.Z.; Resources, D.W. and S.Z.; Data curation, N.L.; Writing—original draft, N.L.; Writing—review & editing, N.L.; Supervision, D.W. and S.Z.; Funding acquisition, D.W. All authors have read and agreed to the published version of the manuscript.

**Funding:** National Natural Science Foundation of China: research on quantitative discrimination of deep coal rock stability (51374009); research on reasonable bearing mechanism and calculation theory of pre-stressed anchor cable compression arch in deep coal roadway (51674005).

**Institutional Review Board Statement:** Not applicable.

**Informed Consent Statement:** Not applicable.

**Data Availability Statement:** Not applicable.

**Conflicts of Interest:** The authors declare no conflict of interest.

## References

1. Zhang, X.; Tang, J.; Pan, Y.; Yu, H. Experimental study on intensity and energy evolution of deep coal and gas outburst. *Fuel* **2022**, *324*, 124484. [\[CrossRef\]](#)
2. Ding, X.; Zhai, C.; Xu, J.; Yu, X.; Sun, Y.; Cong, Y.; Zheng, Y.; Tang, W. Research on the layout optimization and utilization of floor gas extraction roadway: A case study in Shoushan No.1 Coal Mine, China. *Arab. J. Geosci.* **2022**, *15*, 1188. [\[CrossRef\]](#)
3. Cheng, X.; Sun, H. A Data-Driven Fine-Management and Control Method of Gas-Extraction Boreholes. *Processes* **2022**, *10*, 2709. [\[CrossRef\]](#)

4. Zhang, F.; Wang, G.; Wang, B. Study and Application of High-Level Directional Extraction Borehole Based on Mining Fracture Evolution Law of Overburden Strata. *Sustainability* **2023**, *15*, 2806. [[CrossRef](#)]
5. Guo, J.; Zhang, T.; Pan, H.; Wu, J. Experimental investigation of the creep damage evolution of coal rock around gas extraction boreholes at different water contents. *PLoS ONE* **2023**, *18*, e0278783. [[CrossRef](#)]
6. Zhu, M.; Yin, Y.; Peng, C.; Cheng, L.; Hao, Y.; Hou, K.; Zhang, H.; Zhang, J. Analysis of Crustal Stress and Its Influence on the Stability of the Deep Tunnel in the Huanaote Mining Area. *Adv. Civ. Eng.* **2022**, *2022*, 4077305. [[CrossRef](#)]
7. Li, G.; Ma, F.; Guo, J.; Zhao, H.; Liu, G. Study on deformation failure mechanism and support technology of deep soft rock roadway. *Eng. Geol.* **2020**, *264*, 105262. [[CrossRef](#)]
8. Yu, Y.; Chen, D.; Zhao, X.; Wang, X.; Zhang, L.; Zhu, S. Stabilization Mechanism and Safety Control Strategy of the Deep Roadway with Complex Stress. *Adv. Civ. Eng.* **2020**, *2020*, 8829651. [[CrossRef](#)]
9. Matayev, A.; Abdiev, A.; Kydrashov, A.; Musin, A.; Khvatina, N.; Kaumetova, D. Research into technology of fastening the mine workings in the conditions of unstable masses. *Min. Miner. Depos.* **2021**, *15*, 78–86. [[CrossRef](#)]
10. Małkowski, P.; Niedbalski, Z.; Majcherczyk, T.; Bednarek, Ł. Underground monitoring as the best way of roadways support design validation in a long time period. *Min. Miner. Depos.* **2020**, *15*, 1–14. [[CrossRef](#)]
11. Tahmasebinia, F.; Yang, A.; Feghali, P.; Skrzypkowski, K. Structural Evaluation of Cable Bolts under Static Loading. *Appl. Sci.* **2023**, *13*, 1326. [[CrossRef](#)]
12. Tahmasebinia, F.; Yang, A.; Feghali, P.; Skrzypkowski, K. A Numerical Investigation to Calculate Ultimate Limit State Capacity of Cable Bolts Subjected to Impact Loading. *Appl. Sci.* **2022**, *13*, 15. [[CrossRef](#)]
13. Krykovskiy, O.; Krykovska, V.; Skipochna, S. Interaction of rock-bolt supports while weak rock reinforcing by means of injection rock bolts. *Min. Miner. Depos.* **2021**, *15*, 8–14. [[CrossRef](#)]
14. Zhao, Y.; Zhang, J.; Xiang, Z. Research on Arching Mechanism of the Lane Arching under Pre-Stress Bolt Supporting. *Adv. Mater. Res.* **2013**, *671*, 1140–1143. [[CrossRef](#)]
15. Li, G.; Hu, Y.; Tian, S.; Ma, W.; Huang, H. Analysis of deformation control mechanism of prestressed anchor on jointed soft rock in large cross-section tunnel. *Bull. Eng. Geol. Environ.* **2021**, *80*, 9089–9103. [[CrossRef](#)]
16. Li, P.; Chen, Y.; Huang, J.; Wang, X.; Liu, J.; Wu, J. Design principles of prestressed anchors for tunnels considering bearing arch effect. *Comput. Geotech.* **2023**, *156*, 105307. [[CrossRef](#)]
17. Song, Z.; Lei, J.; Wang, X.; Xu, X.; Xin, X. Study on Roadway Parameters of Broken Compound Roof of Gently Inclined Thick Coal Seam. *Energy Procedia* **2012**, *16*, 334–340. [[CrossRef](#)]
18. Kang, H.; Lin, J.; Wu, Y. Development of high pretensioned and intensive supporting system and its application in coal mine roadways. *Procedia Earth Planet. Sci.* **2009**, *1*, 479–485.
19. Cao, F.; Fang, T. Application and Analysis of Bolt Support in Mine Driving Roadway. *Math. Probl. Eng.* **2022**, *2022*, 2521555. [[CrossRef](#)]
20. Wu, Q.; Liu, H.; Dai, B.; Cheng, L.; Li, D.; Qin, P. Influence of Base-Angle Bolt Support Parameters and Different Sections on Overall Stability of a Roadway under a Deeply Buried High Stress Environment Based on Numerical Simulation. *Sustainability* **2023**, *15*, 2496. [[CrossRef](#)]
21. Yan, K.; Wei, J. Parameter Optimization on Bolt Supporting of Deep Roadway Surrounding Rock. *Adv. Mater. Res.* **2013**, *931*, 387–391.
22. Zhang, K.; Su, J.; Liu, Z.; Chen, H.; Zhang, Q.; Sun, S. Sensitivity Analysis and Experimental Verification of Bolt Support Parameters Based on Orthogonal Experiment. *Shock. Vib.* **2020**, *2020*, 8844282. [[CrossRef](#)]
23. Wu, D.; Li, N.; Hu, M.; Liu, H. Study on Formation Mechanism of Pre-stressed Anchor Pressure Arch Based on Safe Co-Mining of Deep Coal and Gas. *Sustainability* **2023**, *15*, 3004. [[CrossRef](#)]
24. Yin, D.; Chen, S.; Ge, Y.; Liu, R. Mechanical properties of rock-coal bi-material samples with different lithologies under uniaxial loading. *J. Mater. Res. Technol.* **2021**, *10*, 322–338. [[CrossRef](#)]
25. Zhao, Z.; Sun, W.; Chen, S.; Ma, Q.; Gao, X.; Zhang, M. Transfer of anchoring load in layered roadway roof under different lithological sequences. *Arab. J. Geosci.* **2018**, *11*, 792. [[CrossRef](#)]
26. Pang, D.; He, K.; Xu, Y.; Chang, J.; Niu, X.; Li, C. Stress Distribution Law of Full-Length Anchorage Bolt in Rectangular Roadway. *Front. Earth Sci.* **2022**, *10*, 885681. [[CrossRef](#)]
27. Li, X.; Wu, B.; Zhu, Y.; Guo, J.; Li, Z. Numerical Study on Deformation and Failure Characteristics of Rectangular Roadway. *Geofluids* **2023**, *2023*, 3792978. [[CrossRef](#)]

**Disclaimer/Publisher’s Note:** The statements, opinions and data contained in all publications are solely those of the individual author(s) and contributor(s) and not of MDPI and/or the editor(s). MDPI and/or the editor(s) disclaim responsibility for any injury to people or property resulting from any ideas, methods, instructions or products referred to in the content.